Changxue Xu¹

Department of Industrial, Manufacturing, and Systems Engineering, Texas Tech University, Lubbock, TX 79409 e-mail: changxue.xu@ttu.edu

Zhengyi Zhang

School of Naval Architecture and Ocean Engineering, Huazhong University of Science and Technology, Wuhan 430074, China e-mail: zhengyizhang@hust.edu.cn

Yong Huang

Department of Mechanical and Aerospace Engineering, University of Florida, Gainesville, FL 32611 e-mail: yongh@ufl.edu

Heqi Xu

Department of Industrial, Manufacturing, and Systems Engineering, Texas Tech University, Lubbock, TX 79409 e-mail: Heqi.Xu@ttu.edu

Phase Diagram of Pinch-off Behaviors During Drop-on-Demand Inkjetting of Alginate Solutions

Viscoelastic polymer solutions have been extensively utilized in inkjet printing for a variety of biomedical applications. The pinch-off of viscoelastic jets is a key step toward the generation of droplets in inkjet printing. This complex process is governed by the interplay of four stresses, including inertial stress, capillary stress, viscous stress, and elastic stress. Depending on polymer solution properties and process conditions, four types of pinch-off phenomenon were observed during inkjetting of viscoelastic alginate solutions. In this study, material properties of alginate solutions with different concentrations have been characterized, and three dimensionless numbers (Ohnesorge number Oh, Deborah number De, and Weber number We) have been proposed to analyze different pinch-off behaviors. The phase diagram in terms of these three dimensionless numbers has been constructed to classify the regimes for different pinch-off types during inkjetting of viscoelastic alginate solutions. It is found that (1) at low De and Oh, the capillary stress is mainly balanced by the inertial stress, resulting in front pinching. (2) At medium De and low Oh, with the increase of We, the pinch-off type may change from front pinching to hybrid pinching to exit pinching. (3) At low Oh and high De, the capillary stress is mainly balanced by the elastic stress, resulting in exit pinching. (4) At high Oh and De, the viscoelastic effect is dominant. With the increase of We, middle pinching turns to be exit pinching due to the increase in the initial ligament diameter near the forming droplet. [DOI: 10.1115/1.4044252]

Keywords: inkjet bioprinting, pinch-off, dimensionless numbers, alginate solutions, biomedical manufacturing

1 Introduction

During the pinch-off process, a fluid jet or ligament thins with time and eventually disintegrates into droplet(s) [1]. Biomaterials widely used in various biomedical applications are viscoelastic in nature. The pinch-off process of viscoelastic polymer solutions is a complex process determined by capillary stress, viscous stress, elastic stress, and inertial stress. Understanding the underlying physics of viscoelastic ligament pinch-off is of great importance for a wide variety of drop-wise applications in tissue engineering and regenerative medicine.

The pinch-off behaviors of viscoelastic jets have been widely investigated in dripping [2], inkjet printing [3-5], and liquid bridge [6-8]. The pinch-off process of viscoelastic polymer jets is typically composed of three consecutive steps: inertio-capillary thinning, elasto-capillary thinning, and finite extensibility. In the inertio-capillary thinning, the two main forces are the capillary force and inertial force. The ligament thinning follows a power-law function of jetting time with an exponent of 2/3 [2]. In the elastocapillary thinning, the polymer molecules are stretched to induce elastic stress, which balances the capillary stress. The ligament thinning follows an exponential function with the jetting time [2,7,8]. In the finite extensibility, the polymer molecules reach the maximum stretching limit. The polymer solution behaves like a very viscous anisotropic Newtonian fluid, which is characterized by the steady extensional viscosity of the polymer solutions. The ligament thinning follows a linear decay [9,10]. Different dimensionless numbers have been utilized to construct phase diagrams with

respect to jetting dynamics [11–13] and impingement [14] of viscoelastic fluids. Zhang et al. [11] constructed a 3D phase diagram based on Weber number, elasto-capillary number, and Ohnesorge number, which includes the effects of both the operating conditions and the polymer solution properties during the laser-induced forward transfer of viscoelastic polymer solutions. Five different jetting regions were classified: no material transfer, well-defined jetting, well-defined jetting with an initial bulgy shape, jetting with a bulgy shape, and pluming/splashing. Hoath et al. [13] used Weissenberg number Wi to classify three different regimes of behavior during inkjet printing of viscoelastic materials. In Region I, the polymer chains were in a relaxed manner and the fluid behaved like a Newtonian fluid. The maximum polymer concentration for good jet formation was scaled with a molecular weight to the power of (1-3v) where v is the solvent quality coefficient. In Region II (1/2 < Wi < polymer chain extensibility), the fluid was viscoelastic, and the maximum polymer concentration was scaled with a molecular weight to the power of (1-6v). In Region III (Wi>L), the polymer chains reached the stretching limit, and the maximum polymer concentration was scaled with a molecular weight to the power of (-2v). Morrison and Harlen [12] used Deborah number to classify six jet behaviors in drop-on-demand (DOD) inkjetting of viscoelastic fluids: single droplet, Newtonian, fewer (larger) satellites, beads-on-a-string, some tail retraction, and bungee. Zhang et al. [14] investigated impingement types and printing quality in laser-induced forward transfer of viscoelastic alginate solutions, and classified three impingement types (droplet-impingement printing, jet-impingement printing with multiple breakups, and jetimpingement printing with single breakup) in a (Weber number, Ohnesorge number, elasto-capillary number) space. However, knowledge of a pinch-off phase diagram is still elusive in DOD inkjetting of viscoelastic fluids.

¹Corresponding author.

Manuscript received May 13, 2019; final manuscript received July 10, 2019; published online July 26, 2019. Editor: Y. Lawrence Yao.

The previous study identified four different types of pinch-off based on the location of the first pinch-off location during inkjet printing of viscoelastic alginate solutions. This paper is a follow-up study to classify the regimes of the four different pinch-off behaviors using dimensionless numbers. The objective of this work is to study the phase diagram of pinch-off behaviors in DOD inkjetting of viscoelastic alginate solutions. DOD inkjet printing has been widely utilized in various biomedical applications because of important advantages, including high resolution, high printing speed, and low cost [15,16]. For the increasing popularity of DODbased three-dimensional (3D) printing technology, this study has selected DOD inkjet printing to study the pinch-off behaviors during printing viscoelastic alginate solutions, which are well accepted for 3D bioprinting and drug delivery. The material properties were controlled by adjusting the polymer concentration, and the process conditions were determined by choosing different excitation voltages. The organization of this paper is as follows. First, the materials and experimental setup are presented. Second, material properties of alginate solutions with different concentrations are characterized and three dimensionless numbers are proposed to investigate pinch-off behaviors. Finally, 2D and 3D phase diagrams based on Ohnesorge, Deborah, and Weber numbers are constructed to classify the regions of the four different pinch-off behaviors in DOD inkjetting of viscoelastic alginate solutions. The resulting knowledge in this paper should be applicable to any dilute (or semidilute) viscoelastic polymer solution utilized in inkjet printing.

2 Materials and Methods

2.1 Materials. Alginate, particularly sodium alginate, has been wildy used as a constituent of bioink [15,17–21] in a variety of 3D bioprinting mimicking the natural extracellular matrix. Sodium algiante has important properties including good biocompatibility, high water content, and low cost [19,20,22]. In addition, alginate can be modified to improve cell adhesion and proliferation [23], and the mechancial properties can be improved [24]. Therefore, sodium alginate solution has been utilzed in this study. The concentrations of the sodium alginate solutions used in this study are 0.10–2.00% (w/v).

2.2 Methods. The DOD inkjet printing system shown in Fig. 1 includes several key components: an inkjet nozzle with an orifice diameter of $120~\mu m$ (MicroFab, Plano, TX), an excitation waveform generator, a pneumatic controller, and a time-resolved imaging system. The nozzle dispenser was used to generate droplets in a DOD mode. The excitation waveform generator was used to generate excitation waveforms applied to the piezoelectric actuator of the nozzle dispenser. The pneumatic controller was used to adjust the backpressure of the fluid reservoir to obtain an ideal meniscus for good droplet formation. The imaging system was used to capture images of the droplet formation process based on a time-revolved

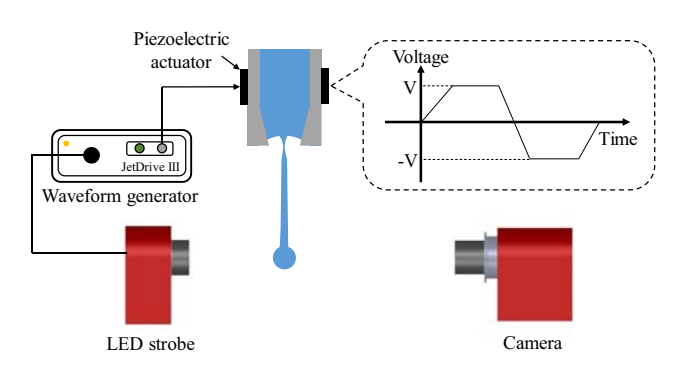


Fig. 1 Experimental setup

imaging method. The resolution of the captured images is 1032×778 pixels, and one pixel (the minimum achievable feature resolution) is $3.2 \,\mu\text{m}$. The jet velocity was determined from the images using the ImageJ software developed by the National Institutes of Health. More details regarding the DOD inkjet printing setup can be found from a previous study [15,16,25].

The typical excitation waveform used for DOD inkjet printing is bipolar shown in Fig. 1, which consists of a succession of positive/ negative square-wave pluses [15,16,26]. For the bipolar waveform, the second pulse of the wave is used to cancel some of the residual acoustic oscillations that may remain in the dispense nozzle after droplet ejection. The bipolar excitation waveform used in the study is defined as follows: excitation voltages in the range of 30-70 V with an interval of 5 V, rise time $3 \mu \text{s}$, fall time $3 \mu \text{s}$, dwell time $30 \mu \text{s}$, echo time $30 \mu \text{s}$, and frequency 50 Hz. More details can be found in previous studies [16,26,27].

3 Property Characterization of Alginate Solutions and Dimensionless Numbers

In order to analyze pinch-off behaviors, the material properties of the sodium alginate solutions with different concentrations were characterized in this section. The density and surface tension were measured in a previous study [1]. The shear viscosity under different shear rates was measured using a rotational rheometer (ARES, TA Instrument, New Castle, DE) in a Couette geometry. It is seen in Fig. 2 that the shear viscosity of the sodium alginate solutions decreases with the increase in the shear rate. This shear-thinning property benefits successful droplet formation of the alginate solutions, especially with high alginate concentrations. However, the shear viscosity does not vary significantly with the shear rate from 50 to 900/s. The zero-shear viscosity is obtained by fitting the measured data using the Carreau-Yasuda model, which represents a nearly constant shear viscosity at low shear rates. In this study, for simplicity, the zero-shear viscosity is adopted to determine the dimensionless numbers.

The longest relaxation time of viscoelastic polymer solutions can be measured using the equation [28]:

$$\frac{D(t)}{D_0} = \left(\frac{G_1 D_0}{4\gamma}\right)^{\frac{1}{3}} e^{-\frac{t}{3\lambda}}$$

where D(t) is the ligament diameter, D_0 is the initial ligament diameter, G_1 is related to the elastic modulus, γ is surface tension, t is the time, and λ is the longest relaxation time. Then, the longest relaxation time was found based on the slope $(-(1/3\lambda))$ of the

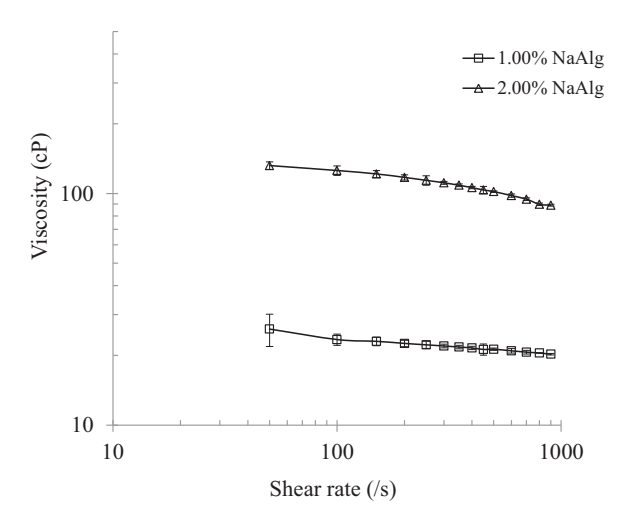


Fig. 2 Shear viscosity of two representative sodium alginate solutions at different shear rates (error bar: \pm one standard deviation)

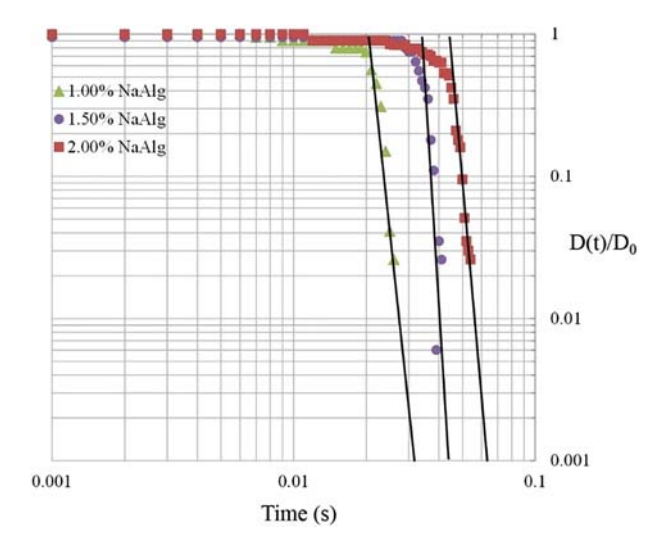


Fig. 3 Longest relaxation time measurement using the 1%, 1.5%, and 2% polymer solutions

log-log plot of (D(t), t) during the pinch-off period shown in Fig. 3. The estimated longest relaxation time has an error within $\pm 5\%$ of its mean value based on the measurement data of the polymer solutions.

The pinch-off behaviors of viscoelastic alginate solutions are determined by the interplay of the capillary, viscous, elastic, and inertial stresses. Three dimensionless numbers are utilized to characterize the effects of these stresses on the droplet formation process: Ohnesorge number (Oh), Deborah number (De), and Weber number (We). Ohnesorge number is defined as Oh = $\mu/\sqrt{\rho R \gamma}$ where μ is shear viscosity, ρ is density, and R is the inkjet nozzle orifice radius. Deborah number is defined as De = λ/τ where τ is the characteristic process time. If the inertial effect is dominant (Oh less than 1 [7,28]), τ is the Rayleigh timescale $\tau_c = \sqrt{\rho R^3/\gamma}$. If the viscous effect is dominant (Oh greater than 1 [7,28]), τ is the visco-capillary timescale $\tau_v = \mu R/\gamma$. Weber number is defined as $We = \rho RU^2/\gamma$ where U is the jet velocity. The rheological properties of the sodium alginate solutions used were measured, and related Ohnesorge number and Deborah number were calculated as given in Table 1.

4 Pinch-off Behaviors in Drop-on-Demand Inkjetting

4.1 Classification of Pinch-off Behaviors in Drop-on- Demand Inkjetting. The sodium alginate solutions are ejected out from the inkjet dispensor to form a ligament due to deformation of the piezoelement. The ligament thins and breaks under the

interplay of the capillary stress, viscous stress, elastic stress, and inertial stress. During the DOD inkjetting of sodium alginate solutions, four different pinch-off behaviors have been reported as shown in Fig. 4 [1]: front pinching, hybrid pinching, exit pinching, and middle pinching. The pinch-off behaviors depend on the material properties of polymer solutions and the process conditions (e.g., excitation voltage).

Figure 4(a) shows the front pinching where the first ligament pinch-off occurs near the forming droplet. Two dominant stresses are the capillary stress and inertial stress, which result in the ligament thinning with a power-law decay. Figure 4(c) shows the exit pinching where the first ligament pinch-off occurs near the inkjet dispenser. Two dominant stresses are the capillary stress and elastic stress, resutling in ligament thinning with exponential decay. In hybrid pinching shown in Fig. 4(b), there are two simultaneous pinch-off locations near both the forming droplet and the inkjet dispenser. Two dominant stresses are the capillary stress and inertial stress, but the elastic stress starts to affect the ligament thinning process. In middle pinching shown in Fig. 4(d), the ligament thins uniformly and breaks up due to Rayleigh instability. The dominant stresses are capillary stress, viscous stress, and elastic stress.

4.2 Discussion on Phase Diagrams. Various phase diagrams have been proposed to define the transition between different modes of interest during the liquid bridge, dripping, various jetting, and spraying, and such phase diagrams are usually constructed based on a space of materials properties, process dynamics, and/or a combination of them. For example, an Oh and De phase diagram was utilized to investigate the BOAS phenomenon during the thinning of the viscoelastic liquid bridge [7], and We and Oh were used to construct phase diagrams to illustrate the transition of dripping and jetting [29]. Weber number, representing the ratio of fluid kinetic energy (operating condition-dependent property) to surface energy (material property-dependent property), is usually selected frequently to represent the printing process in addition to the Capillary and Weissenberg numbers [30]. Unfortunately, the lack of applicable phase diagrams has been a weakness in the field of jetting as pointed out by a recent review article [31].

4.2.1 Two-Dimensional Phase Diagram. Ohnesorge number is defined as the ratio of the viscous stress to the inertial stress and capillary stress. At Oh < 1 the inertial stress is dominant while at Oh > 1 the viscous stress is dominant. Deborah number is defined as a ratio of the polymer's longest relaxation time to the characteristic process time. When the inertial stress is dominant (Oh < 1), the characteristic process time is the Rayleigh timescale. When the viscous stress is dominant (Oh > 1), the characteristic process time is the visco-capillary timescale. The polymer's longest relaxation time represents the elastic stress. Hence, De represents the ratio of the elastic stress to the inertial or viscous stress. Figure 5 shows the De-Oh phase diagram at a given We. It is seen

Table 1 Material properties of the polymer solutions and the related dimensionless values. Adapted with permission from [1]. Copyright © 2017 American Chemical Society.

Sodium alginate concentration (w/v)	Density ρ (g/cm ³)	Average zero-shear viscosity μ (cP)	Surface tension γ (mN/m)	Longest relaxation time $\lambda (\mu s)$	Oh	De
0.10%	1.001	2.8	72.1 ± 0.1	320	0.04	5.84
0.15%	1.002	3.7	71.7 ± 0.3	380	0.06	6.92
0.20%	1.002	4.5	71.5 ± 0.3	390	0.07	7.09
0.25%	1.003	5.5	70.8 ± 0.3	400	0.08	7.23
0.30%	1.004	6.0	69.9 ± 0.8	410	0.09	7.36
0.35%	1.005	6.7	67.4 ± 0.9	420	0.11	7.40
0.50%	1.005	10.2	52.6 ± 1.2	430	0.18	6.69
1.00%	1.010	31.1	47.5 ± 0.2	650	0.58	9.59
1.50%	1.014	75.2	45.7 ± 0.5	920	1.43	9.32
2.00%	1.021	139.5	44.6 ± 0.3	1650	2.67	8.79

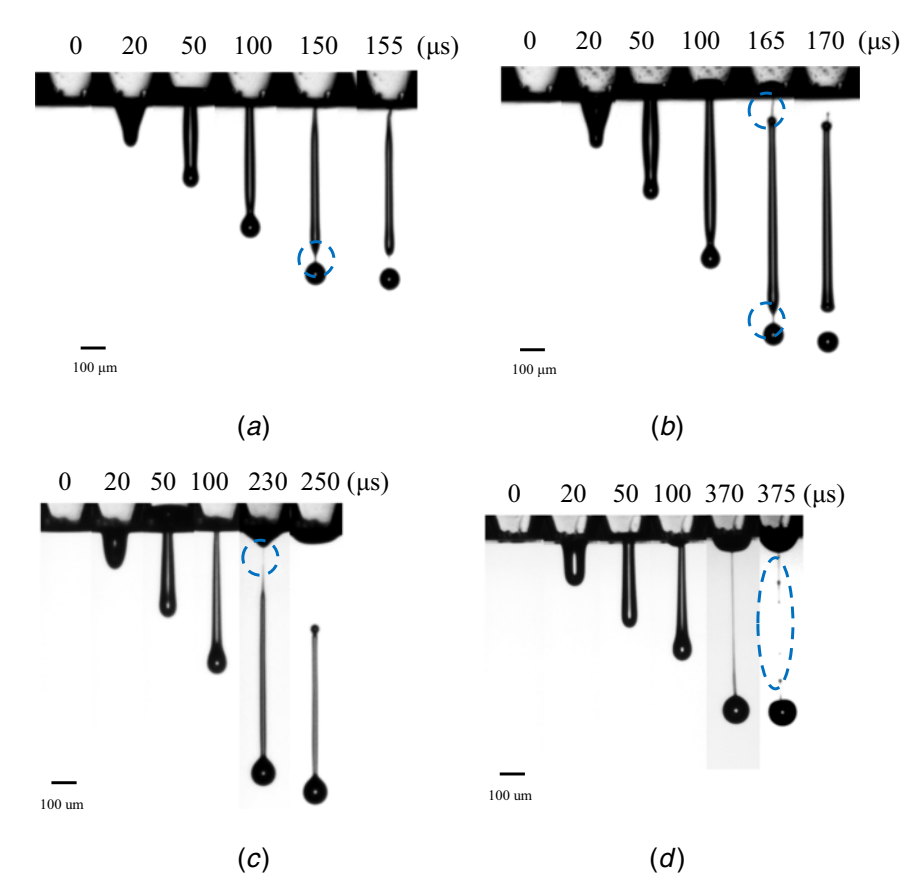


Fig. 4 Four pinch-off behaviors in DOD inkjetting of viscoelastic polymer solutions: (a) front pinching, (b) hybrid pinching, (c) exit pinching, and (d) middle pinching. Pinch-off locations are highlighted [1]. Reprinted with permission from [1]. Copyright © 2017 American Chemical Society.

that Oh is in the range of 0.04–2.67, and De is in the range of 5.84– 9.59, which are determined by the rheological properties of the sodium alginate solutions. In Fig. 5, it shows that the pinch-off types switch between four types of a pinch-off with the increase in De and Oh. At low De and Oh, the viscoelastic effect is small. Two dominant stresses for the ligament pinch-off are the capillary stress and inertial stress, resulting in front pinching. At medium De and low Oh, the capillary stress is still mainly balanced by the inertial stress, but the elastic effect starts to show its effect by delaying the ligament thinning near the front-pinching location. In a critical condition, hybrid pinching is observed when the ligament breaks simultaneously at both locations: near the forming droplet and near the inkjet dispenser. At low Oh and high De, the viscous and inertial effects are small. The capillary stress is mainly balanced by the elastic stress, which results in exit pinching. At high Oh and De, the viscoelastic effect is dominant. The capillary stress is mainly balanced by the viscous stress and elastic stress, which may lead to exit pinching or middle pinching.

The pinch-off behaviors during inkjet printing are affected by not only the material properties represented by De and Oh, but also by the printing conditions (such as the excitation waveform), especially the excitation voltage. We represents the ratio of fluid kinetic energy to surface energy. We significantly affects the pinch-off behaviors through the initial ligament morphology. For example, middle pinching is only observed at small We when the initial ligament diameter is uniform. At high We, middle pinching could not be observed, mainly because the initial ligament diameter is not uniform. For example, typically the ligament diameters near the inkjet dispenser and the forming droplet are smaller. The capillary stress is invesely proportional to the local diameter of the ligament. The ligament thinning near the inkjet dispenser and the forming droplet is usually faster than other locations along the ligament.

Hence, middle pinching is not observed at height We. Hybrid pinching is only observed at We ~ 16.5 in Fig. 5(b), since We affects the initial ligament morphology.

4.2.2 Three-Dimensional Phase Diagram. Apparently, two nondimensional number-based spaces may not be sufficient to fully represent the complex pinch-off behavior during inkjetting. Even for simple constant flow-rate dripping applications, it may need a third nondimensional number such as the Bond number to study dripping dynamics, in particular, for large diameter dripping applications [29,32]. During inkjetting, not only the flow rate is not constant, but also the jetting process is influenced by the external excitation waveforms (such as the magnitudes, durations, dwell times, and rates of rise and fall of the waveform) and the nozzle geometry. While the excitation waveform and nozzle geometry may not directly alter the mechanism of the ligament thinning process, it affects the ejected fluid volume and resultant ligament velocity and diameter, which in turns affect the breakup time as well as pinch-off types.

As such, three nondimensional numbers (We, Oh, and De) are used to characterize the pinch-off behavior during inkjetting: two material property-related numbers (Oh, De) and one process dynamics-related number (We). The Oh and De combination [7,33] is expected to capture the thinning behavior of viscoelastic fluids, and the We number captures the influences of external excitation waveform and nozzle geometry, which directly determine the resulting jetting dynamics. Figure 6 depicts such a (We, Oh, De) phase diagram, illustrating the interaction of the four different stresses on the happening of the aforementioned four types of pinch-off behaviors.

For very low sodium alginate concentrations (e.g., 0.1%-0.2% (w/v)), Oh is smaller than 0.07, demonstrating a negligible

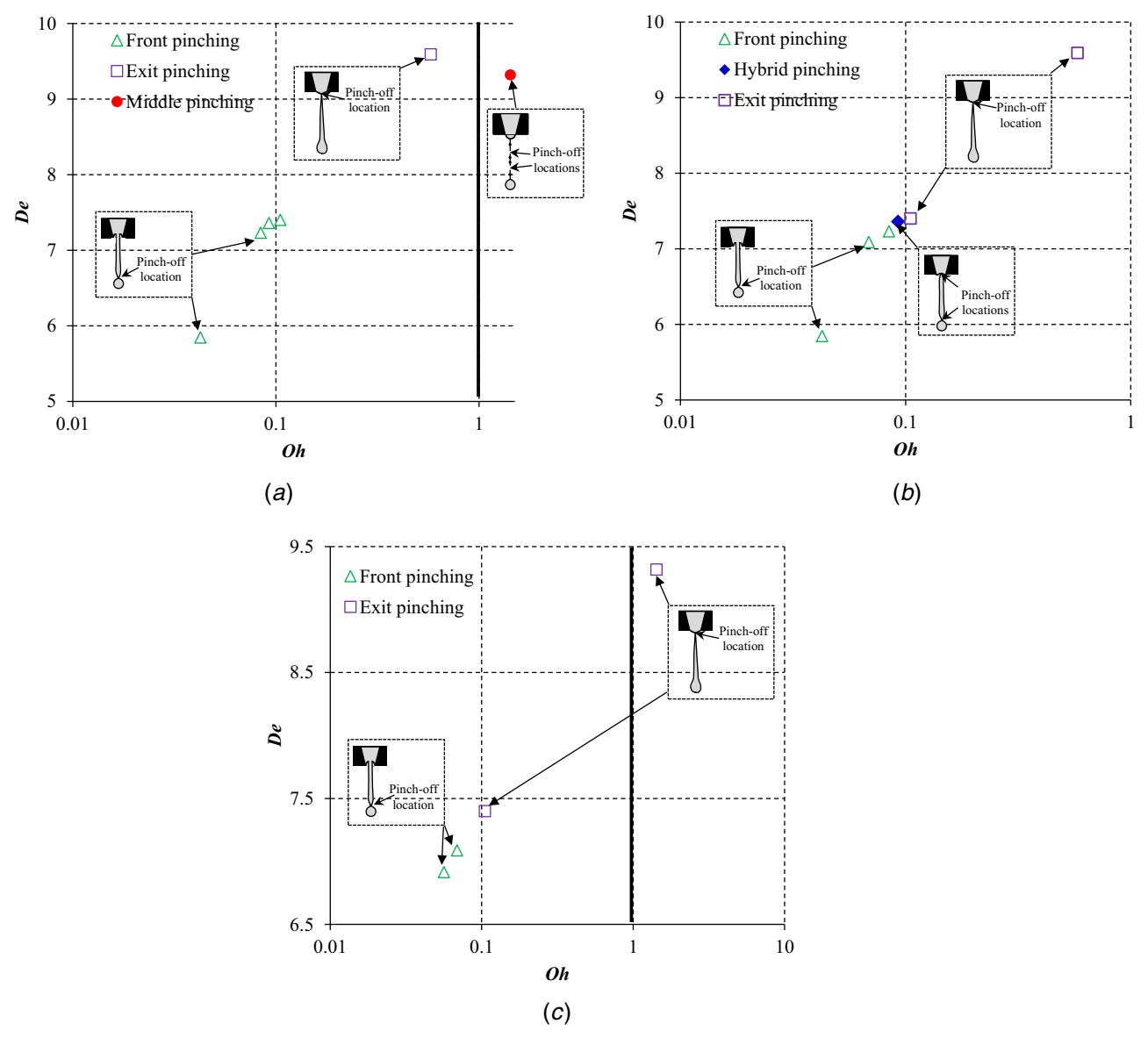


Fig. 5 Pinch-off phase diagram at a given We number range: (a) We \sim 2.50, (b) We \sim 16.50, and (c) We \sim 67.50

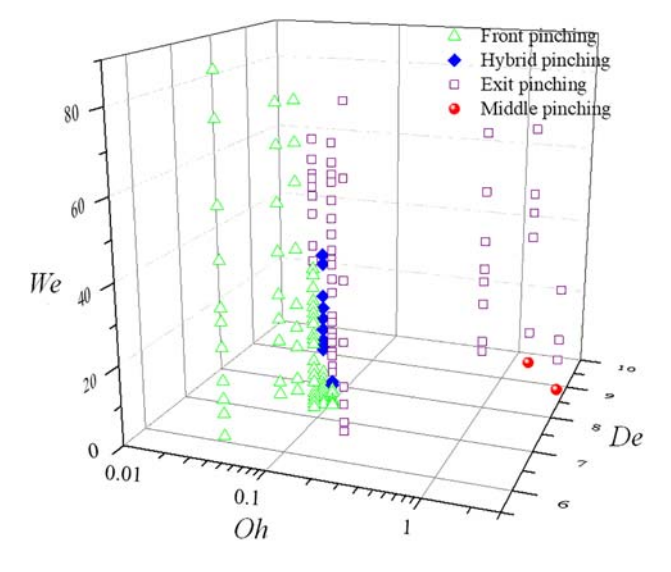


Fig. 6 Pinch-off phase diagram in (We, Oh, De) space

viscous effect. Despite De>1.00, the critical ligament diameter for the elastic stress large enough to balance the capillary stress is around $16 \, \mu \rm m$ for the 0.10% alginate solution compared to the initial ligament diameter of $120 \, \mu \rm m$ [1]. During most of the time of its ligament thinning process, the elastic stress is not large enough to balance the capillary stress. Therefore, both the viscous and elastic effects are negligible, leading to front pinching at the voltage of $30{\text -}70 \, \rm V$.

For low sodium alginate concentrations (e.g., 0.25%–0.35% (w/v)), Oh \leq 0.11 and De > 1.00. The main forces are still inertial and capillary stresses. However, the viscous and elastic effects start playing an important role during ligament thinning. The critical ligament diameter is around 22 μ m for the 0.30% alginate solution compared to the initial ligament diameter of around 120 μ m [1]. The pinch-off type is significantly affected by the fluid kinematics, which determines the initial ligament diameter near the ligament head. With the increase in We, the pinch-off type may change from front pinching to hybrid pinching to exit pinching.

For intermediate sodium alginate concentrations (e.g., 0.5%-1% (w/v)), Oh < 1.00 and De > 1.00, so the elastic effect starts to be dominant during the most time of ligament thinning process. As observed, exit pinching occurs at the voltage range of 30–70 V.

The two main forces are the elastic and capillary stresses. The ligament thinning follows the exponential decay.

For high sodium alginate concentrations (e.g., 1.5%–2% (w/v)), Oh>1.00, and De>1.00, three main stresses are the viscous stress, elastic stress, and capillary stress. At the ligament location near the forming droplet, the capillary stress is balanced the viscous stress and the elastic stress. However, at the location near the inkjet dispenser, the capillary stress is mainly balanced by the elastic stress due to the high-frequency pressure wave. At small We, middle pinching occurs since the fluid of the ligament flows back into the inkjet dispenser and joins the forming droplet. With the increase in We, middle pinching turns to be exit pinching due to the increase in the initial ligament diameter as well as the breakup time at the location near the forming droplet.

5 **Conclusions and Future Work**

This study has investigated different regimes for four types of pinch-off depending on viscoelastic polymer solution properties and process conditions during DOD inkjet printing of alginate solutions. The phase diagram in terms of Oh, De, and We has been constructed to classify these regimes. This study concludes as follows. (1) At low De and Oh, the viscoelastic effect is small. Two main stresses are the capillary stress and the inertial stress, resulting in front pinching. (2) At medium De and low Oh, the capillary stress is still mainly balanced by the inertial stress, but the elastic effect starts to show its effect by delaying the ligament thinning near the front-pinching location. With the increase in We, the pinchoff type may change from front pinching to hybrid pinching to exit pinching. (3) At low Oh and high De, the viscous and inertial effects are small. Two main stresses are the capillary stress and the elastic stress, which results in exit pinching. (4) At high Oh and De, the viscoelastic effect is dominant. The capillary stress is mainly balanced by the viscous and elastic stresses. With the increase in We, middle pinching turns to be exit pinching due to the increase in the initial ligament diameter.

Future work may include (1) computational modeling of ligament thinning process, and (2) effects of different types of pinch-off on the following droplet formation behaviors including droplet size, velocity, and satellite droplets.

Funding Data

• The work was partially supported by the National Science Foundation (Grant Nos. CMMI-1314834, CMMI-1634755 and CMMI-1762282; Funder ID: 10.13039/501100008982).

References

- [1] Xu, C., Zhang, Z., Fu, J., and Huang, Y., 2017, "Study of Pinch-off Locations During Drop-on-Demand Inkjet Printing of Viscoelastic Alginate Solutions," Langmuir, 33(20), pp. 5037-5045.
- [2] Tirtaatmadja, V., McKinley, G. H., and Cooper-White, J. J., 2006, "Drop Formation and Breakup of low Viscosity Elastic Fluids: Effects of Molecular Weight and Concentration," Phys. Fluids, 18(4), p. 043101.
- [3] Vadillo, D., Tuladhar, T., Mulji, A., Jung, S., Hoath, S., and Mackley, M., 2010, "Evaluation of the Inkjet Fluid's Performance Using the "Cambridge Trimaster' Filament Stretch and Break-up Device," J. Rheol., **54**(2), pp. 261–282.
- [4] Ardekani, A., Sharma, V., and McKinley, G., 2010, "Dynamics of Bead Formation, Filament Thinning and Breakup in Weakly Viscoelastic Jets," J. Fluid Mech., **665**, pp. 46–56.
- [5] Oliveira, M. S., and McKinley, G. H., 2005, "Iterated Stretching and Multiple Beads-on-a-String Phenomena in Dilute Solutions of Highly Extensible Flexible Polymers," Phys. Fluids, **17**(7), p. 071704.
- [6] Anna, S. L., and McKinley, G. H., 2001, "Elasto-capillary Thinning and Breakup of Model Elastic Liquids," J. Rheol., 45(1), pp. 115-138.

- [7] Bhat, P. P., Appathurai, S., Harris, M. T., Pasquali, M., McKinley, G. H., and Basaran, O. A., 2010, "Formation of Beads-on-a-String Structures During Break-up of Viscoelastic Filaments," Nat. Phys., 6(8), pp. 625-631.
- [8] Clasen, C., Eggers, J., Fontelos, M. A., Li, J., and McKinley, G. H., 2006, "The Beads-on-String Structure of Viscoelastic Threads," J. Fluid Mech., 556,
- [9] Clasen, C., Bico, J., Entov, V., and McKinley, G., 2009, "Gobbling Drops': the Jetting-Dripping Transition in Flows of Polymer Solutions," J. Fluid Mech., 636, pp. 5-40.
- [10] Entov, V., and Hinch, E., 1997, "Effect of a Spectrum of Relaxation Times on the Capillary Thinning of a Filament of Elastic Liquid," J. Non-Newtonian Fluid Mech., 72(1), pp. 31-53.
- [11] Zhang, Z., Xiong, R., Mei, R., Huang, Y., and Chrisey, D. B., 2015, "Time-resolved Imaging Study of Jetting Dynamics During Laser Printing of Viscoelastic Alginate Solutions," Langmuir, 31(23), pp. 6447–6456.
- [12] Morrison, N. F., and Harlen, O. G., 2010, "Viscoelasticity in Inkjet Printing," Rheol. Acta, 49(6), pp. 619–632.
- [13] Hoath, S. D., Harlen, O. G., and Hutchings, I. M., 2012, "Jetting Behavior of Polymer Solutions in Drop-on-Demand Inkjet Printing," J. Rheol., 56(5), pp. 1109-1127.
- [14] Zhang, Z., Xiong, R., Corr, D. T., and Huang, Y., 2016, "Study of Impingement Types and Printing Quality During Laser Printing of Viscoelastic Alginate Solutions," Langmuir, 32(12), pp. 3004-3014.
- [15] Xu, C., Chai, W., Huang, Y., and Markwald, R. R., 2012, "Scaffold-Free Inkjet Printing of Three-Dimensional Zigzag Cellular Tubes," Biotechnol. Bioeng., 109(12), pp. 3152-3160.
- [16] Xu, C., Zhang, M., Huang, Y., Ogale, A., Fu, J., and Markwald, R. R., 2014, "Study of Droplet Formation Process During Drop-on-Demand Inkjetting of Living Cell-Laden Bioink," Langmuir, 30(30), pp. 9130-9138.
- [17] Murphy, S. V., Skardal, A., and Atala, A., 2013, "Evaluation of Hydrogels for bio-Printing Applications," J. Biomed. Mater. Res., Part A, 101(1), pp. 272-284.
- [18] Ding, H., Tourlomousis, F., and Chang, R., 2018, "A Methodology for Quantifying Cell Density and Distribution in Multidimensional Bioprinted Gelatin-Alginate Constructs," ASME J. Manuf. Sci. Eng., 140(5), p. 051014.
- [19] Nishiyama, Y., Nakamura, M., Henmi, C., Yamaguchi, K., Mochizuki, S., Nakagawa, H., and Takiura, K., 2009, "Development of a Three-Dimensional Bioprinter: Construction of Cell Supporting Structures Using Hydrogel and State-of-the-art Inkjet Technology," ASME J. Biomech. Eng., 131(3), p. 035001.
- [20] Zhang, Z., Xu, C., Xiong, R., Chrisey, D. B., and Huang, Y., 2017, "Effects of Living Cells on the Bioink Printability During Laser Printing," Biomicrofluidics, 11(3), p. 034120.
- [21] Xu, H., Zhang, Z., and Xu, C., 2019, "Sedimentation Study of Bioink Containing Living Cells," J. Appl. Phys., 125(11), p. 114901.
- [22] Zhang, Z., Chai, W., Xiong, R., Zhou, L., and Huang, Y., 2017, "Printing-induced Cell Injury Evaluation During Laser Printing of 3T3 Mouse Fibroblasts,' Biofabrication, 9(2), p. 025038.
- [23] Alsberg, E., Kong, H., Hirano, Y., Smith, M., Albeiruti, A., and Mooney, D., 2003, "Regulating Bone Formation via Controlled Scaffold Degradation," J. Dent. Res., **82**(11), pp. 903–908.
- [24] Krishnamoorthy, S., Zhang, Z., and Xu, C., 2019, "Biofabrication of Three-Dimensional Cellular Structures Based on Gelatin Methacrylate— Alginate Interpenetrating Network Hydrogel," J. Biomater. Appl., 33(8), pp. 1105-1117.
- [25] Zhang, M., Krishnamoorthy, S., Song, H., Zhang, Z., and Xu, C., 2017, "Ligament Flow During Drop-on-Demand Inkjet Printing of Bioink Containing Living Cells," J. Appl. Phys., 121(12), p. 124904.
- [26] Xu, C., Zhang, Z., Christensen, K., Huang, Y., Fu, J., and Markwald, R. R., 2014, "Freeform Vertical and Horizontal Fabrication of Alginate-Based Vascular-Like Tubular Constructs Using Inkjetting," ASME J. Manuf. Sci. Eng., 136(6), p. 061020.
- [27] Wu, D., and Xu, C., 2018, "Predictive Modeling of Droplet Formation Processes in Inkjet-Based Bioprinting," ASME J. Manuf. Sci. Eng., 140(10), p. 101007. [28] McKinley, G. H., 2005, "Visco-elasto-capillary Thinning and Break-up of
- Complex Fluids," Br. Soc. Rheol., pp. 1-48.
- [29] Ambravaneswaran, B., Subramani, H. J., Phillips, S. D., and Basaran, O. A., 2004, "Dripping-jetting Transitions in a Dripping Faucet," Phys. Rev. Lett., 93(3), p. 034501
- [30] Clasen, C., Phillips, P. M., and Palangetic, L., 2012, "Dispensing of Rheologically Complex Fluids: the map of Misery," AIChE J., 58(10),
- [31] Basaran, O. A., Gao, H., and Bhat, P. P., 2013, "Nonstandard Inkjets," Annu. Rev. Fluid Mech., 45, pp. 85-113.
- [32] Subramani, H. J., Yeoh, H. K., Suryo, R., Xu, Q., Ambravaneswaran, B., and Basaran, O. A., 2006, "Simplicity and Complexity in a Dripping Faucet," Phys. Fluids, 18(3), p. 032106.
- [33] Zhang, Z., Jin, Y., Yin, J., Xu, C., Xiong, R., Christensen, K., Ringeisen, B. R., Chrisey, D. B., and Huang, Y., 2018, "Evaluation of Bioink Printability for Bioprinting Applications," Appl. Phys. Rev., 5(4), p. 041304.